Synthetic Bessel light needle for extended depth-of-field microscopy

Jiamiao Yang, Lei Gong, Yuecheng Shen, and Lihong V. Wang

Citation: Appl. Phys. Lett. **113**, 181104 (2018); doi: 10.1063/1.5058163
View online: https://doi.org/10.1063/1.5058163
View Table of Contents: http://aip.scitation.org/toc/apl/113/18
Published by the American Institute of Physics

Synthetic Bessel light needle for extended depth-of-field microscopy

Jiamiao Yang,[1] Lei Gong,[2] Yuecheng Shen,[1] and Lihong V. Wang[1,a)]
[1]*Caltech Optical Imaging Laboratory, Andrew and Peggy Cherng Department of Medical Engineering, Department of Electrical Engineering, California Institute of Technology, Pasadena, California 91125, USA*
[2]*Department of Optics and Optical Engineering, University of Science and Technology of China, Hefei, Anhui 230026, China*

(Received 17 September 2018; accepted 20 October 2018; published online 2 November 2018)

An ultra-long light needle is highly desired in optical microscopy for its ability to improve the lateral resolution over a large depth of field (DOF). However, its use in image acquisition usually relies on mechanical raster scanning, which compromises between imaging speed and stability and thereby restricts imaging performance. Here, we propose a synthetic Bessel light needle (SBLN) that can be generated and scanned digitally by complex field modulation using a digital micromirror device. In particular, the SBLN achieves a 45-fold improvement in DOF over its counterpart Gaussian focus. Further, we apply the SBLN to perform motionless two-dimensional and three-dimensional microscopic imaging, achieving both improved resolution and extended DOF. Our work is expected to open up opportunities for potential biomedical applications. *Published by AIP Publishing.* https://doi.org/10.1063/1.5058163

Conventional three-dimensional (3D) microscopy suffers from a limited depth of field (DOF), which is determined by the focal depth of the imaging objective lens. High-resolution imaging can be achieved only near the focal plane of the objective, and the lateral resolution decreases rapidly with the distance from the focal plane. Thus, scanning an object or an illuminating beam along the depth direction is required to maintain the resolution at different depths, which negatively impacts the imaging speed.

To extend the DOF of optical microscopy, various methods have been proposed, such as wavefront coding,[1] deconvolution,[2] layer-by-layer frequency domain imaging,[3] and light needles.[4–7] Among them, light needles were most widely used in laser scanning microscopy, such as two-photon microscopy,[8,9] optical coherence tomography,[10,11] light sheet microscopy,[12,13] and photoacoustic microscopy (PAM).[14,15] In particular, the unique self-healing property of a Bessel beam based light needle can enable imaging with an improved penetration depth inside scattering media.[16,17] Nevertheless, their use in image acquisition usually relies on mechanical raster scanning, which limits imaging speed and stability.

Here, we propose a non-diffracting synthetic Bessel light needle (SBLN) to extend the microscope's DOF. The SBLN is synthesized by two scanned symmetrical plane waves generated by a single digital micromirror device (DMD). Such a virtual light needle can be flexibly synthesized at any position by digital means, paving the way for scanning-free imaging. In particular, under the same numerical-aperture (NA) objective, the SBLN achieves a 45-fold improvement in DOF over a focused Gaussian beam. Furthermore, we apply the SBLN to acquire two-dimensional (2D) or 3D microscopy images without mechanical scanning, achieving the extended DOF.

A light needle is essentially a point light on each transverse plane, and a point light can be regarded as a superposition of sinusoidal fringes according to Fourier optics.[18] Therefore, the light needle can be synthesized by the superposition of a series of nondiffracting sinusoidal fringes (NSFs), as illustrated in Fig. 1. By fully exploiting the diffraction-free nature of plane waves, we further propose to create the NSF by the interference of two symmetrically incident plane waves [Fig. 1(a)]. As a result, scanning the two symmetrical plane waves in k-space can synthesize the nondiffracting light needle [Figs. 1(b) and 1(c)], and its intensity distribution in the Cartesian coordinates (x, y, z) can be expressed as

$$I_{\text{needle}}(x,y,z) = \iint\limits_{k_x^2+k_y^2<k_{\max}^2} |E_1(x,y,z)+E_2(x,y,z)|^2 dk_x dk_y, \quad (1)$$

where $E_1 = A\exp[i(k_x x + k_y y + k_z z)]$ and $E_2 = A\exp[i(-k_x x - k_y y + k_z z)]$. A is the amplitude of the two plane waves, and k_x, k_y, and k_z are the components of the wave vector. In practice, the maximum wavenumber, $k_{\max}$, of the two plane waves is limited by the NA of the illumination objective lens: $k_{\max} = \text{NA}\cdot 2\pi/\lambda$, where λ is the wavelength. The kernel $|E_1(x,y,z) + E_2(x,y,z)|^2$ indicates the component interference pattern used to synthesize the light needle.

If the constant background and scaling factors are neglected, the intensity distribution can be mathematically simplified using cylindrical coordinates (r, θ, z) to

$$I_{\text{needle}}(r,\theta,z) = \frac{2\pi^2 \text{NA}}{\lambda r} J_1\left(\frac{4\pi r \text{NA}}{\lambda}\right), \quad (2)$$

where $J_1(\cdot)$ is the first-order Bessel function of the first kind. Thus, we call this nondiffracting focused beam as the synthetic Bessel light needle. It can be seen from Eq. (2) that the SBLN theoretically has an unlimited length in the z direction, an invariant diameter, and constant irradiance along the needle. In fact, the length of the SBLN is determined by the overlap of the two collimated beams after the objective in

a)Author to whom correspondence should be addressed: LVW@caltech.edu.

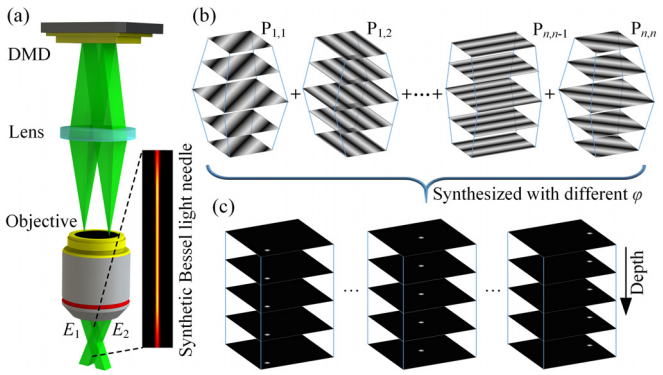

FIG. 1. Principle of the SBLN. (a) The SBLN is synthesized by a series of nondiffracting sinusoidal fringes (NSFs), which are created by the interference of two symmetrically incident plane waves E_1 and E_2. The two plane waves E_1 and E_2 are produced and scanned by a DMD using complex field modulation. (b) $P_{1,1}$, $P_{1,2}$,$\cdots$, $P_{n,n-1}$, and $P_{n,n}$ are the intensity distributions of a series of NSFs with different spatial frequencies k_x and k_y. (c) The SBLN can be synthesized at any position by adding an initial phase φ to E_1.

the experiment. Nevertheless, the achievable length of the SBLN is much greater than the DOF of the objective.

In particular, the SBLN can be synthesized at any spatial position (x_0, y_0) by adding a phase $\varphi = -2k_x x_0 - 2k_y y_0$ to E_1 for each k value, whose intensity profile reads

$$I'_{\text{needle}}(x,y,z) = \iint_{k_x^2+k_y^2<k_{\max}^2} \left| \exp\left[i(-2k_x x_0 - 2k_y y_0)\right] E_1(x,y,z) + E_2(x,y,z) \right|^2 dk_x dk_y = I_{\text{needle}}(x - x_0, y - y_0, z). \quad (3)$$

Thus, such a light needle can be flexibly scanned by digital means, which enables the SBLN-based imaging to be realized without mechanical scanning.

To form and scan two symmetrical plane waves, a single DMD based complex field encoding method[19,20] was utilized, as illustrated in Fig. 2(a). According to the desired amplitude and phase of the interference field of two symmetrical plane waves, the corresponding binary hologram is generated using the super-pixel method, as shown in Fig. 2(b). By switching the binary holograms, these two plane waves were rapidly scanned in k-space, and a series of NSFs were formed at the focal plane of the objective to synthesize the light needle. Figure 2(c) presents the intensity profiles of a generated NSF with $k_x = k_y = 10\pi/L$ at different depths. The NA of the objective is 0.1, and the size $(L \times L)$ of the NSF is $180 \times 180\ \mu\text{m}^2$. Our complex field modulation enables us to maintain its profile over a depth of 3 mm. Conventionally, amplitude-only modulation is adopted for the binary DMD. In this manner, the generated fringe blurs quickly away from the focal plane.

By the superposition of a series of NSFs with different k values, the SBLN can be created. Here, 90×90 k values were scanned to synthesize the light needle. Figure 3(a) shows the SBLN obtained at the center of the NSF. Four *en face* cross-sections were taken from the SBLN to show the profiles of the foci at different depths. For further analysis, the full width at half maximum (FWHM) of the foci along both x and y directions throughout the volume was calculated, which are illustrated in Figs. 3(b) and 3(c), respectively. The volume indicated by white color is the resolution invariant area, where the FWHM reaches 1.9 μm. The SBLN achieves a much larger DOF over a focused Gaussian beam. For a quantitative comparison, we define the DOF of the SBLN as the axial range within which the lateral size increases by up to a factor of $\sqrt{2}$ from the focal value. As a result, the DOF of the SBLN at the center of the NSF is 2500 μm, which is 45-fold longer than that of a Gaussian focus.

For the purpose of imaging, we built an SBLN-based microscope using a photodiode (PDA36A, Thorlabs, Inc.) as a detector, which is sketched in Fig. 4(a). A continuous-wave laser with a wavelength of 532 nm was used as the light source. During the image acquisition, the two symmetric beams were rapidly scanned by switching the binary holograms displayed on the DMD. At the focal plane of the objective (NA = 0.1), these two scanned beams interfered

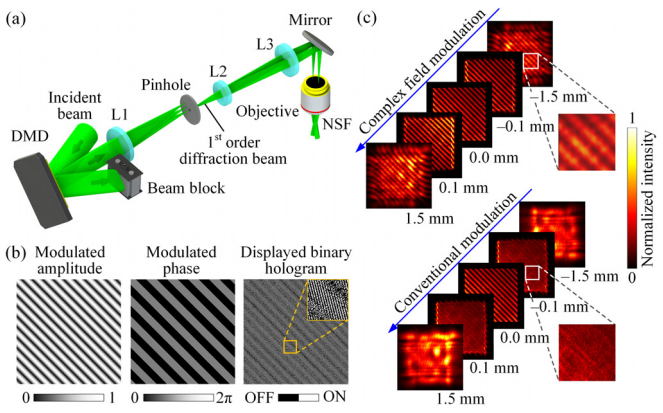

FIG. 2. Generation of NSFs by a DMD. (a) Schematic illustration of the experimental setup. L: lenses. (b) The amplitude and phase distributions of the interference field of two symmetrical plane waves and its corresponding binary hologram designed by the super-pixel method. (c) The intensity profiles of a fringe at different depths generated by our complex field (both the amplitude and the phase) modulation and conventional (amplitude-only) modulation, respectively.

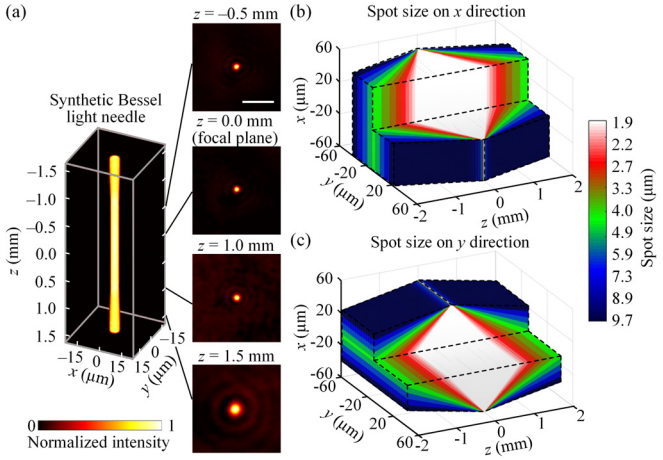

FIG. 3. Synthetic Bessel light needle and its characteristics. (a) Experimentally generated SBLN and four corresponding synthesized foci at different depths of −0.5, 0.0, 1.0, and 1.5 mm. The focal plane is located at $z = 0.0$ mm. (b) and (c) Varying spot sizes of the synthesized foci at different positions in x and y directions, respectively. *Scale bars*, 15 μm.

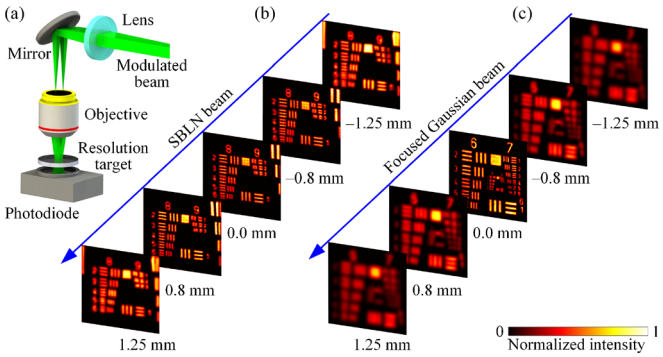

FIG. 4. SBLN-based imaging of a USAF resolution target with an extended DOF. (a) Illustration of the SBLN microscope. (b) and (c) Resolution target imaging at different depths by the SBLN beam and the focused Gaussian beam, respectively.

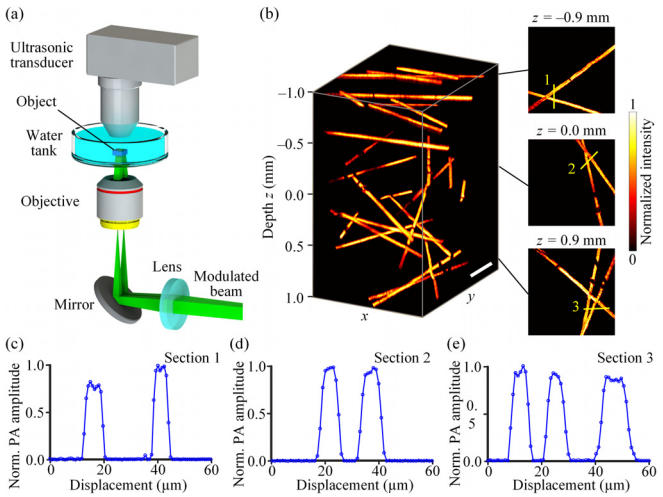

FIG. 5. Volumetric imaging of spatially distributed carbon fibers by SBLN PAM. (a) Illustration of the SBLN photoacoustic microscope. (b) Volume-rendered imaging of the 3D object and three *en face* image slices taken at different depths of −0.9, 0.0, and 0.9 mm. (c)–(e) Corresponding line profiles across the carbon fibers to show its essentially unchanged lateral resolution over the depth range. *Scale bar*, 150 μm.

and formed an SBLN to illuminate a USAF resolution target that served as the object. The field of view (FOV) of the microscope, determined by the size of the NSF, was $180 \times 180\ \mu m^2$.

Figures 4(b) and 4(c) show the reconstructed images of the resolution target placed at different depths acquired by the SBLN and the focused Gaussian beam, respectively. The results show that the features of element 6 in group 8 with a resolution of 456.1 line pairs per mm can be resolved by SBLN microscopy whenever the object is located in the range of −0.8 mm to 0.8 mm. When the imaging depth reaches ±1.25 mm, a slightly decreased resolution is observed, which coincides with the theoretically predicted resolution degradation with a factor of $\sqrt{2}$. In contrast, when the focused Gaussian beam was adopted,[21] the features of element 3 in group 6 (resolution of 80.6 line pairs per mm) are hardly resolved at an imaging depth of ±0.8 mm. When the imaging depth reaches ±1.25 mm, all the patterns in groups 6 and 7 (lowest resolution of 64.0 line pairs per mm) become blurred beyond recognition [Fig. 4(c)]. Overall, SBLN microscopy achieves an extended DOF.

Furthermore, the SBLN was applied to realize volumetric imaging by introducing photoacoustic (PA) detection,[22,23] which is sketched in Fig. 5(a). The depth information was resolved by the time-of-flight information carried by the PA signals. A pulsed laser with a wavelength of 532 nm was used as the light source. A 3D object made of spatially distributed carbon fibers with a diameter around 7 μm was imaged. The object was located in a tank filled with water, and an ultrasonic transducer was fixed above the object to detect the PA signals. The ultrasonic waves were coupled by the water. Here, a montage strategy based on the movement of the object in the horizontal direction was adopted to obtain a larger image. Figure 5(b) shows the volume-rendered image of the object with an area of $600 \times 600 \times 2000\ \mu m^3$. As expected, we obtained high-resolution imaging throughout the volume. Three *en face* image slices were taken at different depths to show its essentially unchanged lateral resolution along the depth. The corresponding line profiles across the carbon fibers are shown in Figs. 5(c)–5(e). All the fibers can be clearly resolved even when they are located at the ends of the depth range ($z = -0.9$ mm or $z = 0.9$ mm). Compared to the conventional PAM using a focused Gaussian beam, our SBLN-based PAM greatly increases the DOF, achieving motionless volumetric imaging. Combined with the contour-scanning method,[24] the SBLN-based PAM can realize high-speed motionless volumetric imaging for features of interest.

In summary, we have proposed and implemented an ultra-long SBLN with a DMD. The SBLN achieves a 45-fold improvement in DOF over the counterpart Gaussian focus. Since the SBLN can be synthesized at any position within the FOV, it is capable of performing direct 2D or 3D image acquisition without mechanical scanning. We applied the SBLN to perform 2D and 3D motionless imaging, achieving an extended DOF in microscopy. This extended DOF and the motionless imaging method are expected to open up opportunities for potential biomedical applications. Additionally, the approach proposed here could be readily adapted for other imaging modalities, for example, light-sheet microscopy[25] and structured-illumination microscopy.[26]

The authors acknowledge financial support from National Institutes of Health (NIH) Grant Nos. DP1 EB016986 (NIH Director's Pioneer Award), R01 NS102213 (PEDBRAIN), U01 NS090579 (BRAIN1 Initiative), and U01 NS099717 (BRAIN2 Initiative).

[1]S. C. Tucker, W. T. Cathey, and E. R. Dowski, Opt. Express **4**, 467 (1999).
[2]F. Aguet, D. Van De Ville, and M. Unser, IEEE Trans. Image Process. **17**, 1144 (2008).
[3]J. Yang, L. Gong, X. Xu, P. Hai, Y. Shen, Y. Suzuki, and L. V. Wang, Nat. Commun. **8**, 780 (2017).
[4]C.-C. Sun and C.-K. Liu, Opt. Lett. **28**, 99 (2003).
[5]H. Wang, L. Shi, B. Lukyanchuk, C. Sheppard, and C. T. Chong, Nat. Photonics **2**, 501 (2008).
[6]M. Zhu, Q. Cao, and H. Gao, JOSA A **31**, 500 (2014).
[7]C. Gohn-Kreuz and A. Rohrbach, Optica **4**, 1134 (2017).
[8]G. Thériault, Y. De Koninck, and N. McCarthy, Opt. Express **21**, 10095 (2013).

[9]G. Thériault, M. Cottet, A. Castonguay, N. McCarthy, and Y. De Koninck, Front. Cell. Neurosci. **8**, 139 (2014).
[10]K.-S. Lee and J. P. Rolland, Opt. Lett. **33**, 1696 (2008).
[11]D. Lorenser, C. C. Singe, A. Curatolo, and D. D. Sampson, Opt. Lett. **39**, 548 (2014).
[12]T. A. Planchon, L. Gao, D. E. Milkie, M. W. Davidson, J. A. Galbraith, C. G. Galbraith, and E. Betzig, Nat. Methods **8**, 417 (2011).
[13]P. J. Keller, A. D. Schmidt, A. Santella, K. Khairy, Z. Bao, J. Wittbrodt, and E. H. Stelzer, Nat. Methods **7**, 637 (2010).
[14]J. Shi, L. Wang, C. Noordam, and L. V. Wang, J. Biomed. Opt. **20**, 116002 (2015).
[15]B. Jiang, X. Yang, and Q. Luo, Opt. Express **24**, 20167 (2016).
[16]F. O. Fahrbach, P. Simon, and A. Rohrbach, Nat. Photonics **4**, 780 (2010).
[17]F. O. Fahrbach, V. Gurchenkov, K. Alessandri, P. Nassoy, and A. Rohrbach, Opt. Express **21**, 13824 (2013).
[18]J. W. Goodman, *Introduction to Fourier Optics* (Roberts and Company Publishers, 2005).
[19]S. A. Goorden, J. Bertolotti, and A. P. Mosk, Opt. Express **22**, 17999 (2014).
[20]J. Yang, Y. Shen, Y. Liu, A. S. Hemphill, and L. V. Wang, Appl. Phys. Lett. **111**, 201108 (2017).
[21]J. Yang, L. Qiu, W. Zhao, Y. Shen, and H. Jiang, Opt. Lett. **39**, 830 (2014).
[22]L. V. Wang, Nat. Photonics **3**, 503 (2009).
[23]L. V. Wang and S. Hu, Science **335**, 1458 (2012).
[24]C. Yeh, B. T. Soetikno, S. Hu, K. I. Maslov, and L. V. Wang, J. Biomed. Opt. **19**, 096011 (2014).
[25]B.-C. Chen, W. R. Legant, K. Wang, L. Shao, D. E. Milkie, M. W. Davidson, C. Janetopoulos, X. S. Wu, J. A. Hammer, and Z. Liu, Science **346**, 1257998 (2014).
[26]P. Kner, B. B. Chhun, E. R. Griffis, L. Winoto, and M. G. L. Gustafsson, Nat. Methods **6**, 339 (2009).